Supplementary materials

Enhanced Acetylene Semi-hydrogenation on Subsurface Carbon Tailored Ni-Ga Intermetallic Catalyst

Xiaohu Ge,[a,#] Zhouhong Ren,[b,#] Yueqiang Cao,[*a] Xi Liu,[b] Jing Zhang,[a] Gang Qian,[a] Xueqing Gong,[c] Liwei Chen,[b] Xinggui Zhou,[a] Weikang Yuan,[a] Xuezhi Duan[*a]

[a] *State Key Laboratory of Chemical Engineering, East China University of Science and Technology, 130 Meilong Road, Shanghai 200237, China*

[b] *School of Chemistry and Chemical Engineering, In-situ Center for Physical Sciences, Frontiers Science Center for Transformative Molecules, Shanghai Jiao Tong University, Shanghai 200240, China*

[c] *Key Laboratory for Advanced Materials, Centre for Computational Chemistry and Research Institute of Industrial Catalysis, East China University of Science and Technology, 130 Meilong Road, Shanghai 200237, China*

[#] *These authors contributed equally to this work.*

[*]*Corresponding Authors: yqcao@ecust.edu.cn; xzduan@ecust.edu.cn*

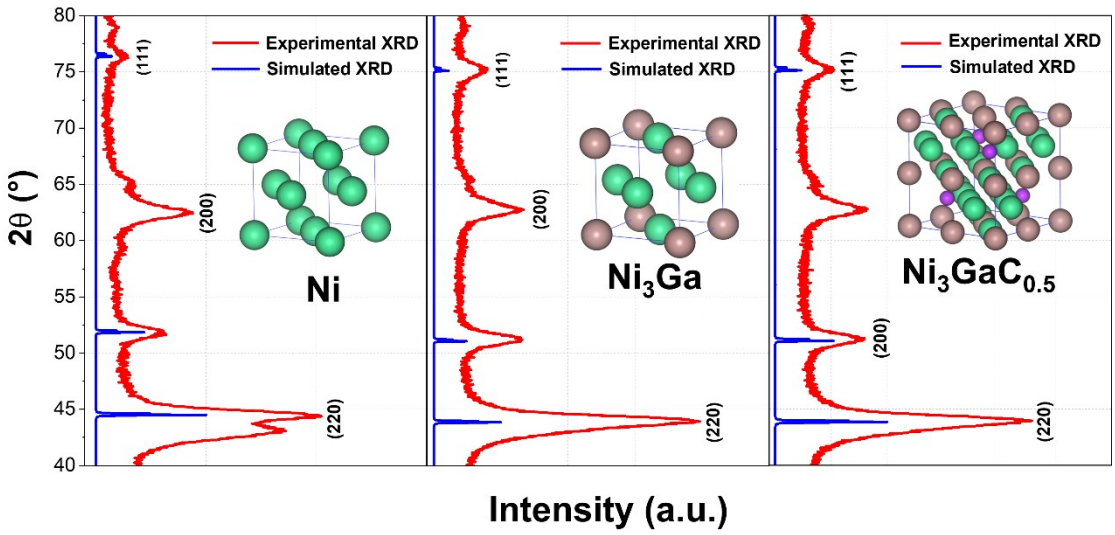

Fig. S1. Comparison for experimental and simulated XRD patterns of the Ni, Ni_3Ga and $Ni_3GaC_{0.5}$ catalysts.

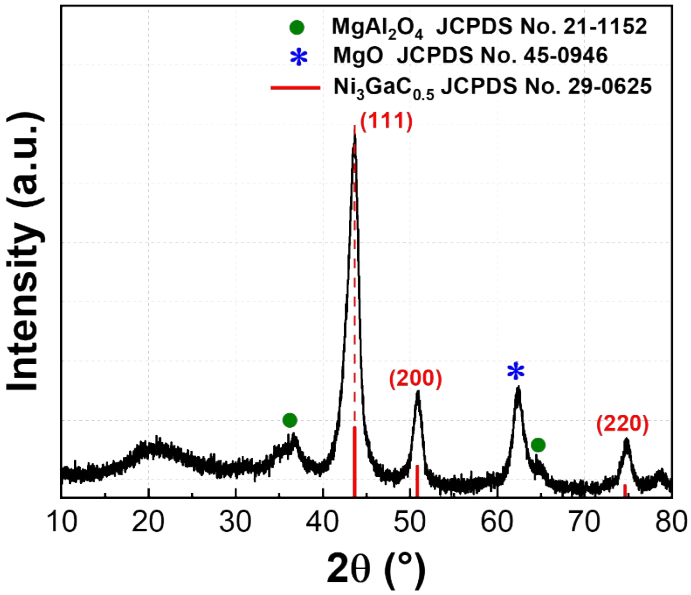

Fig. S2. XRD pattern of the $Ni_3GaC_{0.5}$ catalyst.

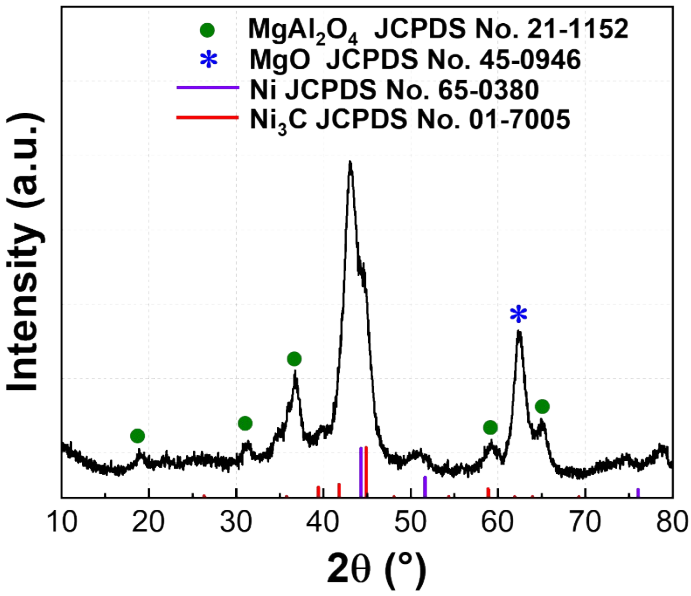

Fig. S3. XRD pattern of the Ni catalyst treated at 300 ^{o}C under 1.0% C_2H_2/N_2 atmosphere for 3h.

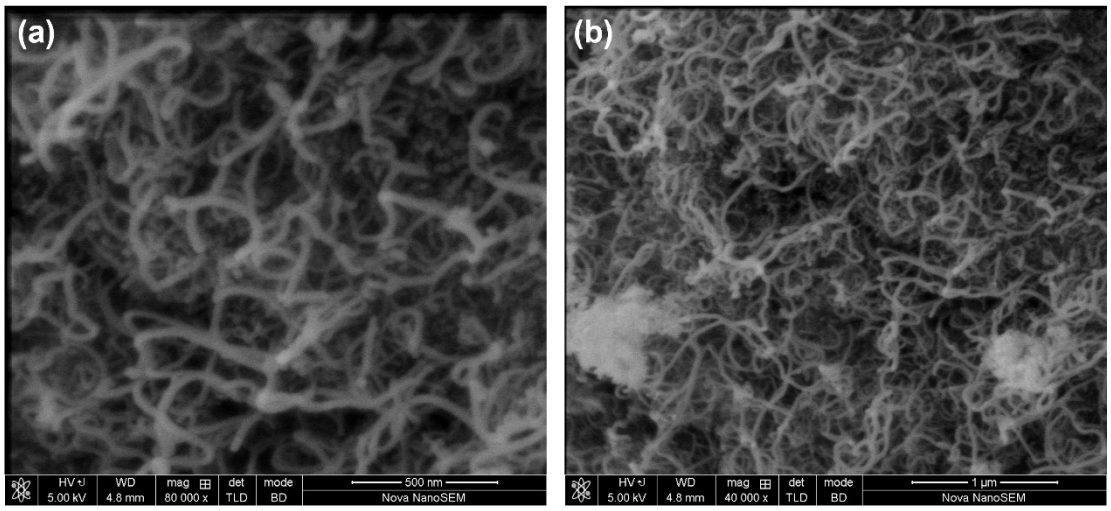

Fig. S4. SEM image of the Ni catalyst treated at 500 ^{o}C under 1.0% C_2H_2/N_2 atmosphere for 3h.

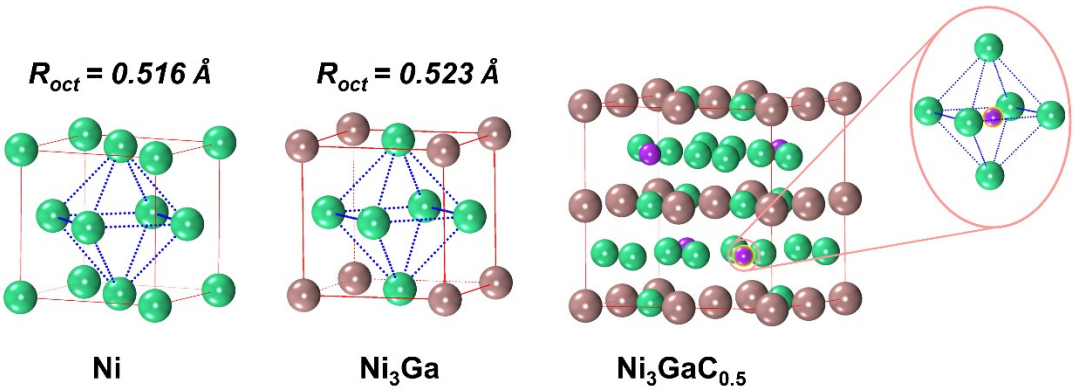

Fig. S5. The optimized structures of bulk Ni, Ni_3Ga and $Ni_3GaC_{0.5}$. R_{oct} is the calculated radius of octahedral site in the corresponding face-centered cubic crystals.

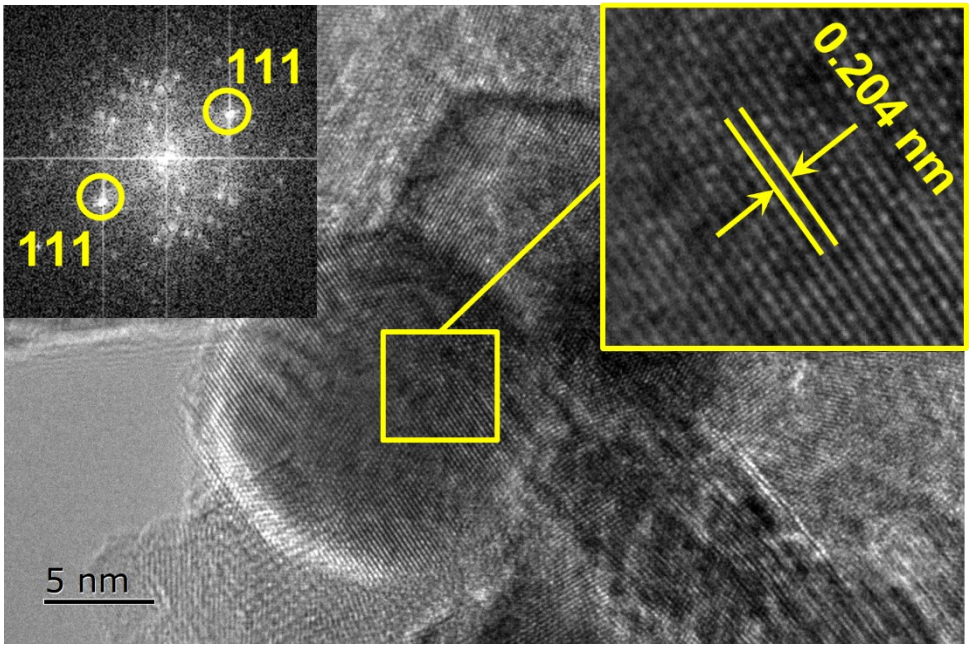

Fig. S6. HRTEM images of the Ni catalyst, where the inset is the corresponding FFT patterns.

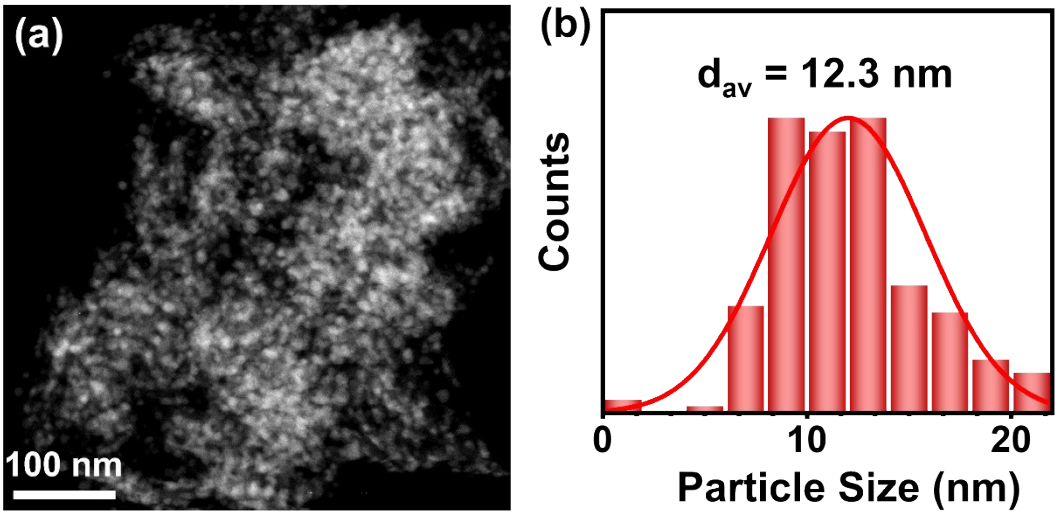

Fig. S7. (a) HAADF-STEM images of the Ni catalyst and (b) the corresponding histogram of the particle size distributions.

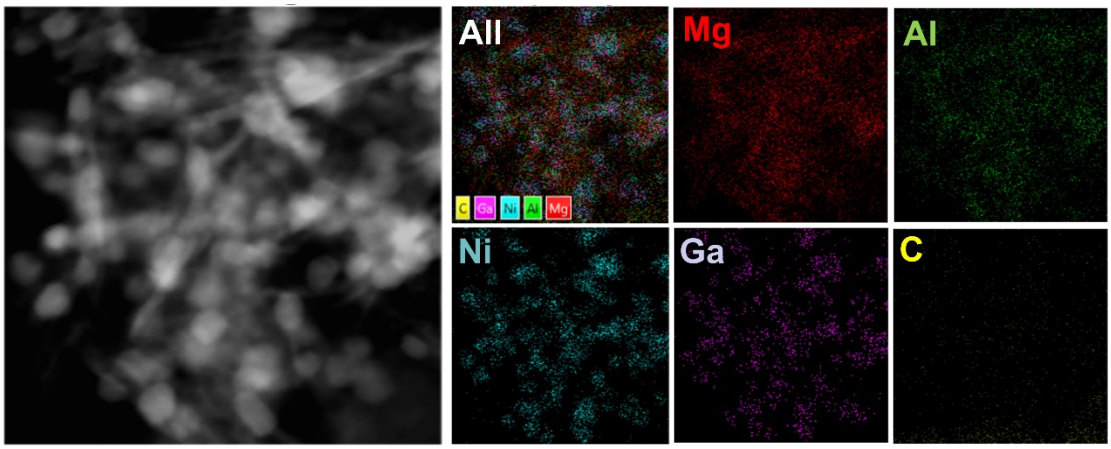

Fig. S8. HAADF-STEM EDS mapping of the Ni_3Ga catalyst.

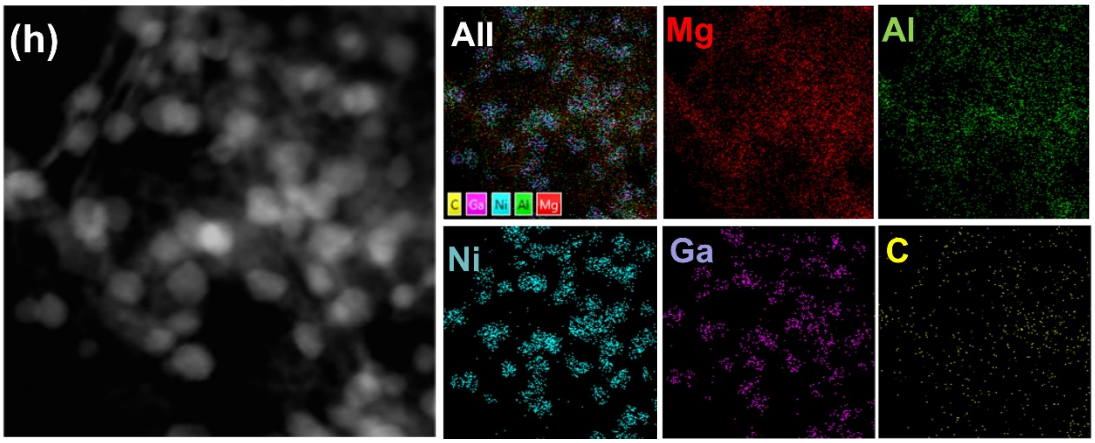

Fig. S9. HAADF-STEM EDS mapping of the $Ni_3GaC_{0.5}$ catalyst.

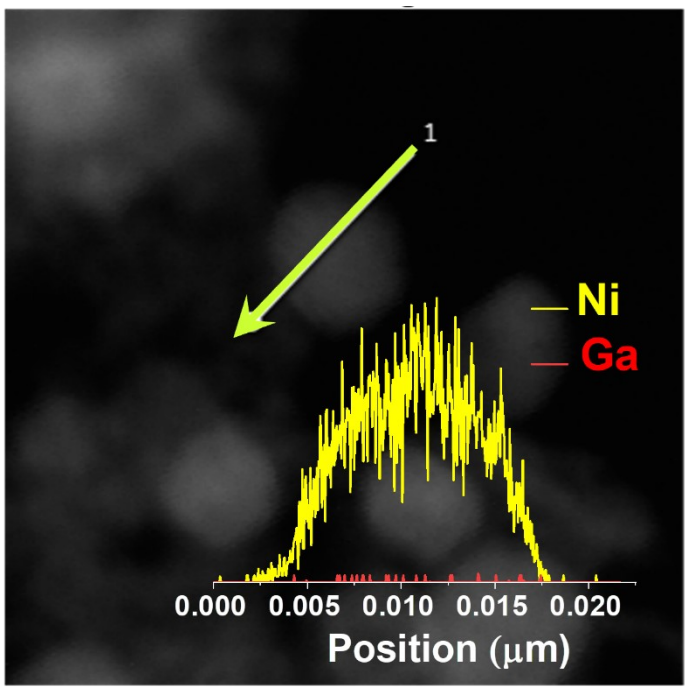

Fig. S10. HAADF-STEM images of the Ni catalyst, in which the insets are the corresponding EDS line-scanning profile analysis.

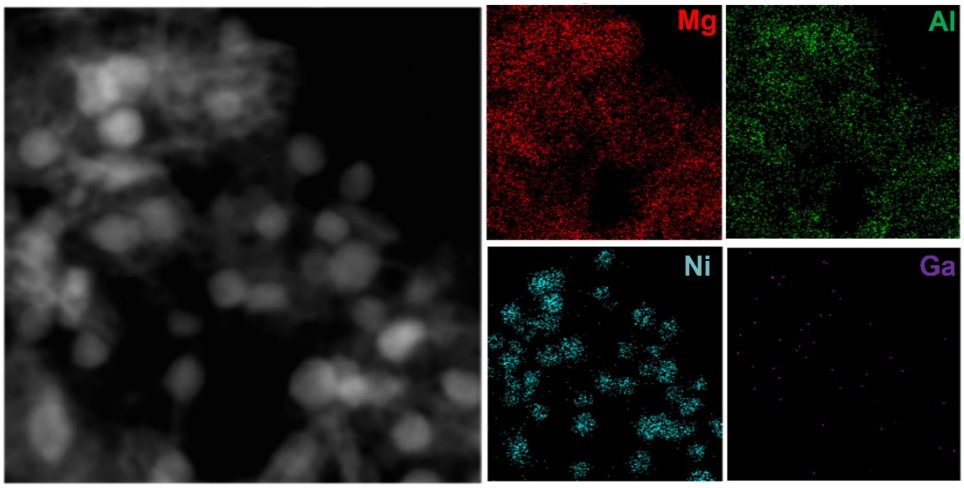

Fig. S11. HAADF-STEM EDS mapping of the Ni catalyst.

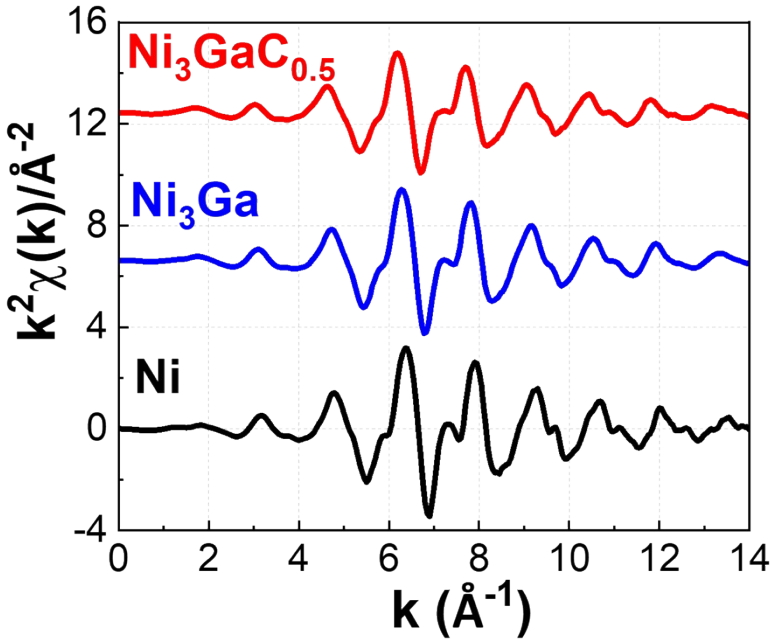

Fig. S12. The EXAFS oscillation functions at the Ni K-edge of Ni, Ni_3Ga and $Ni_3GaC_{0.5}$ catalysts.

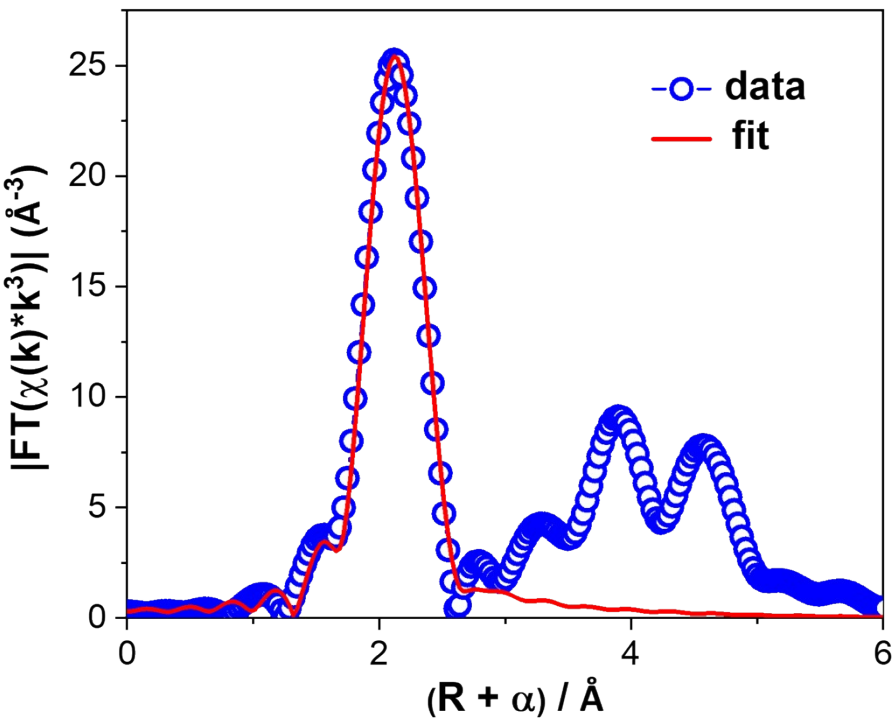

Fig. S13. Fourier transforms of the experimental and fitted EXAFS spectra of Ni at Ni K-edge.

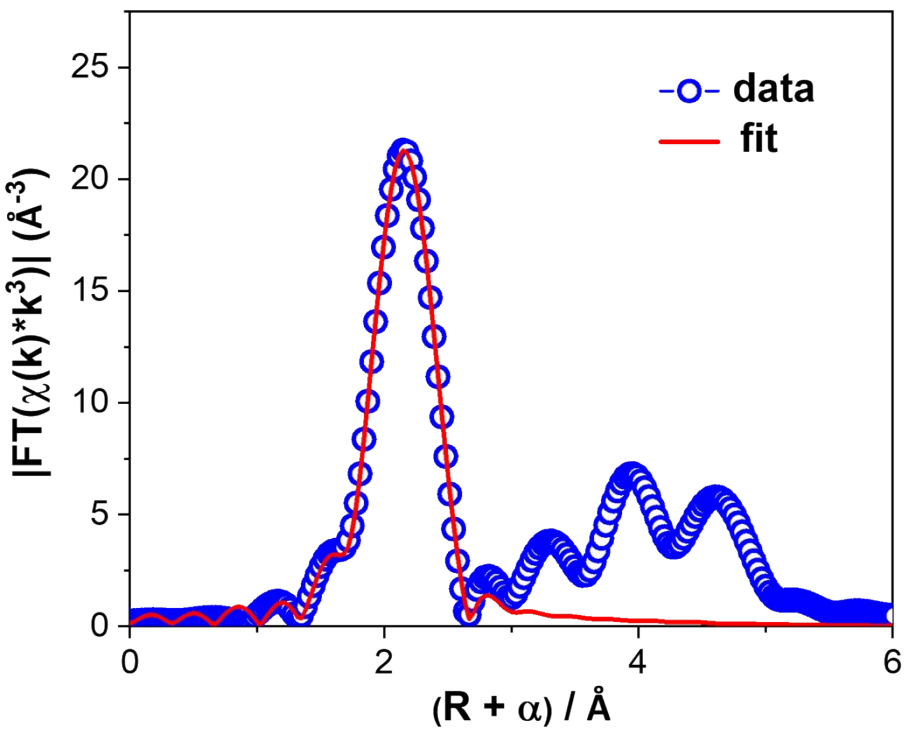

Fig. S14. Fourier transforms of the experimental and fitted EXAFS spectra of Ni_3Ga at Ni K-edge.

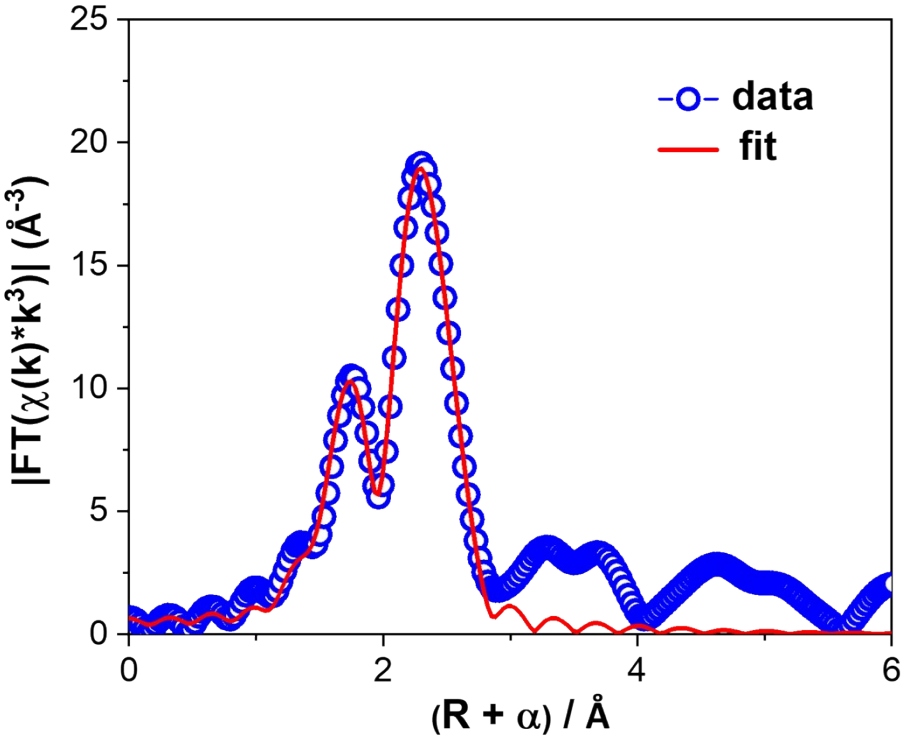

Fig. S15. Fourier transforms of the experimental and fitted EXAFS spectra of $Ni_3GaC_{0.5}$ at Ni K-edge.

Table S1. Structural parameters of Ni, Ni_3Ga and $Ni_3Gac_{0.5}$ from the EXAFS fitting.

Sample	Shell	N[a]	R[b]	ΔE_0 (eV)[c]	σ^2(10^{-3} Å^2)[d]	R factor[e]
Ni	Ni-Ni	10.3±1.6	2.49±0.03	7.4±0.8	4.1±0.4	0.009
Ni_3Ga	Ni-Ni	7.5±1.1	2.52±0.02	6.3±1.4	6.5±0.7	0.007
	Ni-Ga	4.3±1.3	2.54±0.01	8.1±1.5	5.4±1.1	
$Ni_3GaC_{0.5}$	Ni-Ni	6.5±1.5	2.53±0.02	6.5±0.9	3.5±0.5	0.005
	Ni-Ga	3.1±1.4	2.54±0.03	5.7±2.2	7.7±1.4	
	Ni-C	1.5±0.9	1.84±0.01	7.9±0.6	4.2±0.8	

[a]N is coordination number; [b]R is the internal atomic distance; [c]ΔE_0 is the edge-energy shift; [d]σ^2 is Debye-Waller factor; [e]R-factor represents the fitness of data processing.

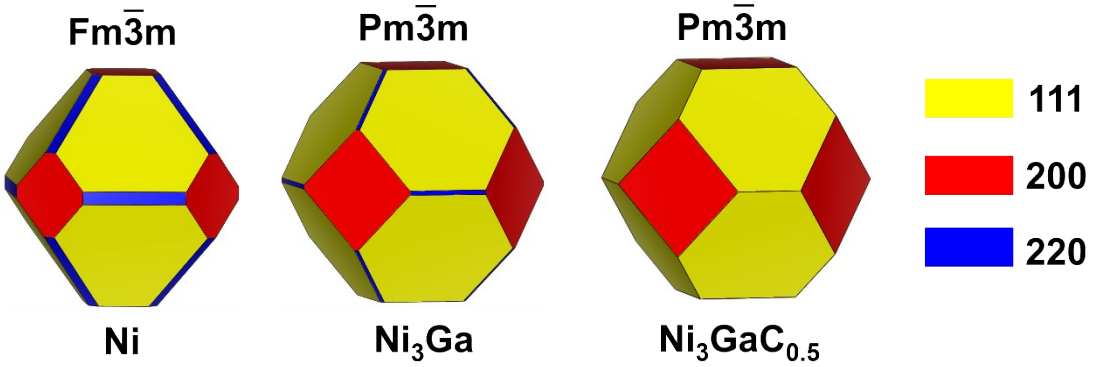

Fig. S16. Wulff crystals for Ni, Ni_3Ga and $Ni_3GaC_{0.5}$ crystallites, where the crystal facets denoted by Miller indices are shown by different color.

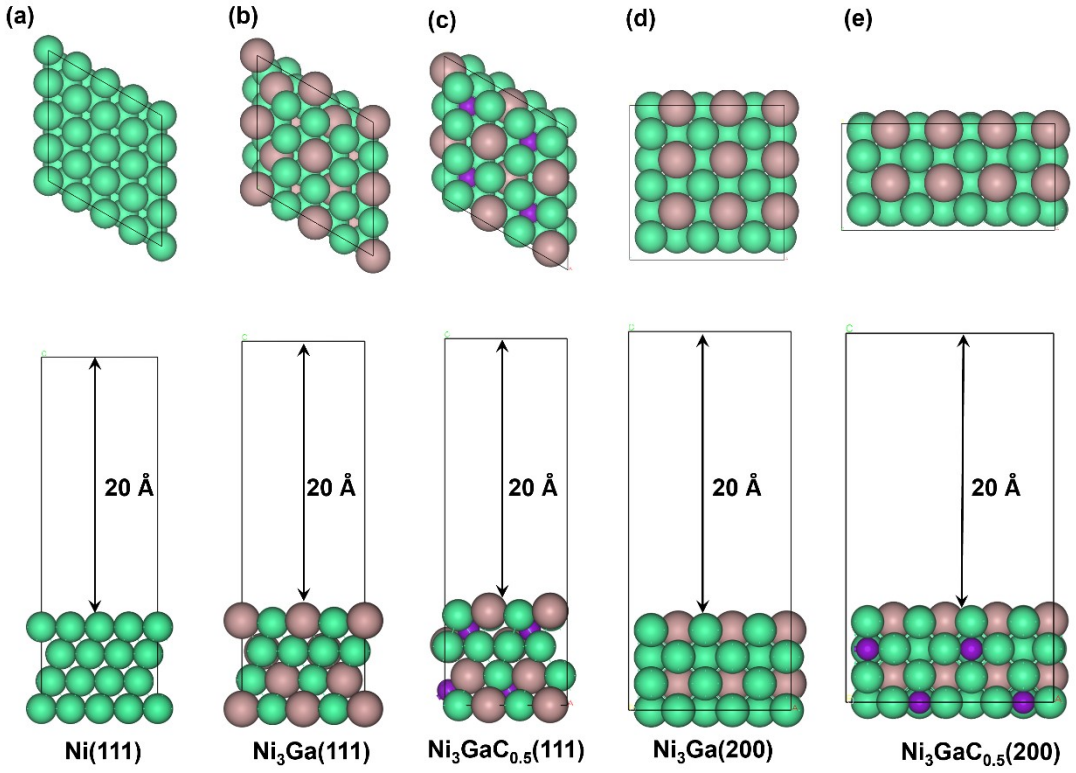

Fig. S17. Schematical illustrations of (a) Ni (111), (b) Ni_3Ga (111), (c) $Ni_3GaC_{0.5}$ (111), (d) Ni_3Ga (200) and (e) $Ni_3GaC_{0.5}$ (200) surfaces.

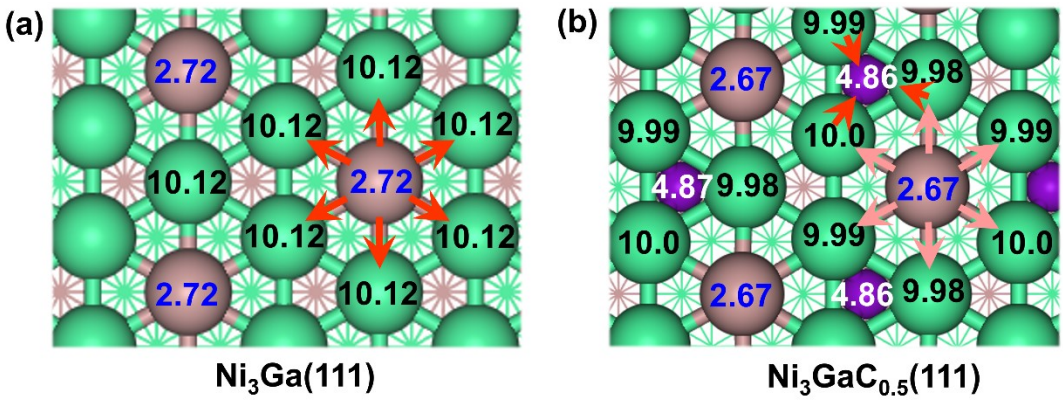

Fig. S18. Bader charge analysis of (a) Ni_3Ga (111) and (b) $Ni_3GaC_{0.5}$ (111) surfaces, the numbers of valence electrons were labeled (Ni in black, Ga in blue and C in white) on the atoms, the unit of the data is electron (e). The arrows point out the electron transfer direction.

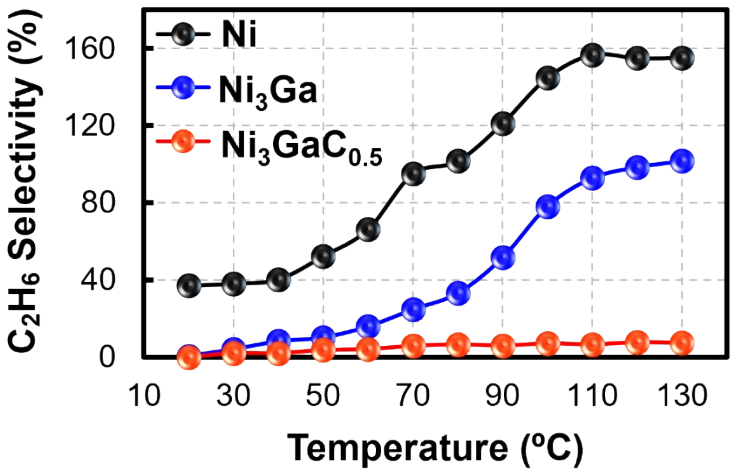

Fig. S19. C_2H_6 selectivity as a function of reaction temperature over the Ni, Ni_3Ga and $Ni_3GaC_{0.5}$ catalysts.

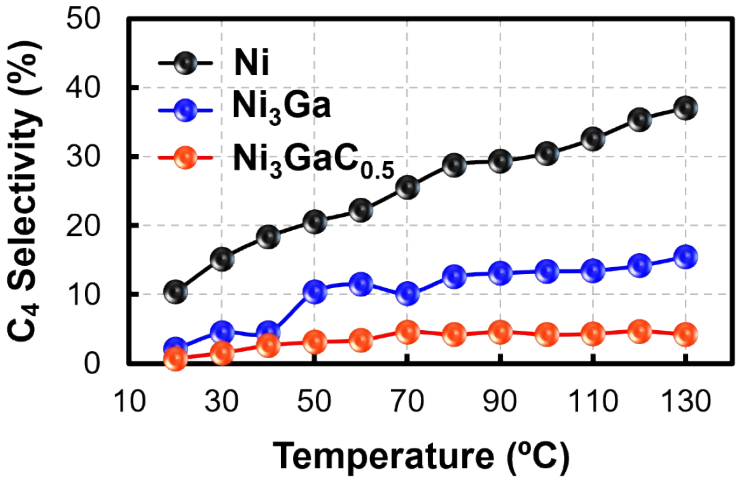

Fig. S20. C_4 selectivity as a function of reaction temperature over the Ni, Ni_3Ga and $Ni_3GaC_{0.5}$ catalysts.

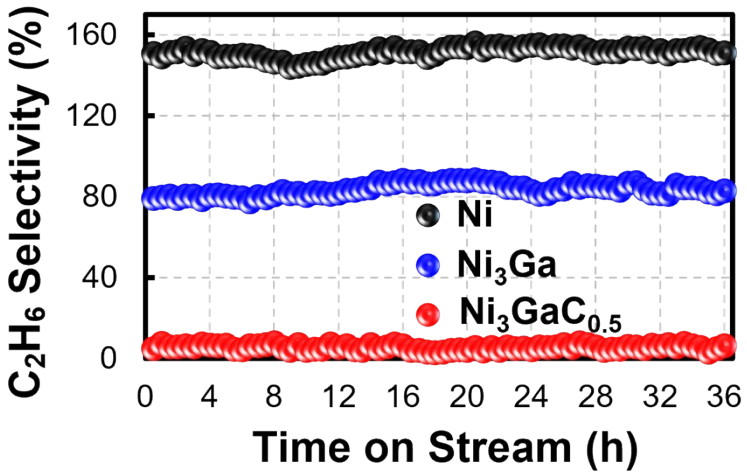

Fig. S21. C_2H_6 selectivity with time on stream over the Ni, Ni_3Ga and $Ni_3GaC_{0.5}$ catalysts.

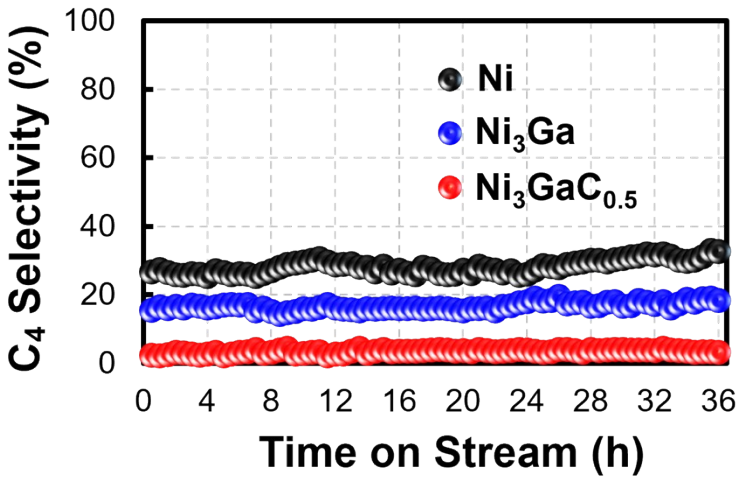

Fig. S22. C_4 selectivity with time on stream over the Ni, Ni_3Ga and $Ni_3GaC_{0.5}$ catalysts.

Table S2. Adsorption energies (E_{ads}/eV) and Gibbs free adsorption energies (G_{ads}/eV) of C_2H_2 on the $Ni_3GaC_{0.5}$ (111) surface.

Top View	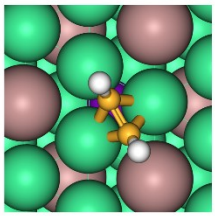	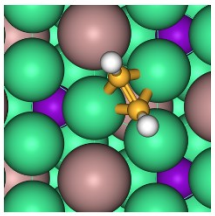	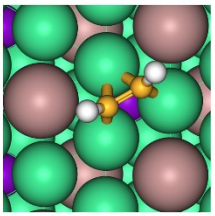	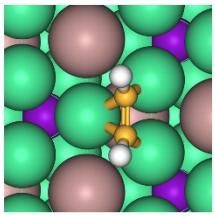
Side View	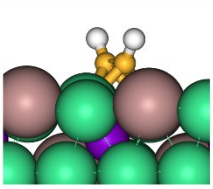	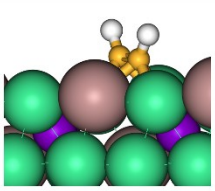	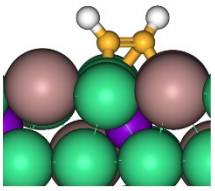	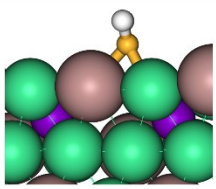
E_{ads} (eV)	**-1.14**	**-2.03**	**-1.16**	**-1.84**
G_{ads} (eV)	**-0.83**	**-1.71**	**-0.84**	**-1.52**

Table S3. Adsorption energies (E_{ads}/eV) and Gibbs free adsorption energies (G_{ads}/eV) of C_2H_4 on the $Ni_3GaC_{0.5}$ (111) surface.

Top View	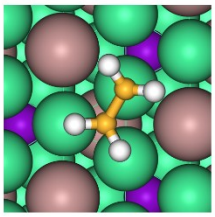
Side View	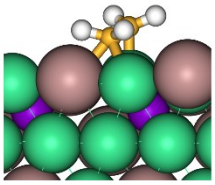
E_{ads} (eV)	**-0.88**
G_{ads} (eV)	**-0.68**

Table S4. Adsorption energies (E_{ads}/eV) and Gibbs free adsorption energies (G_{ads}/eV) of C_2H_2 on the Ni_3Ga (111) surface.

Top View	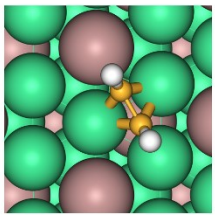	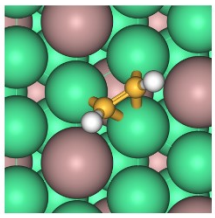	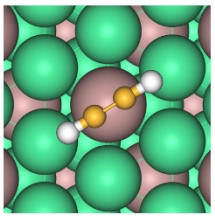
Side View	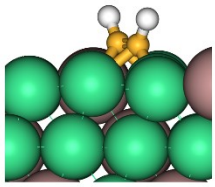	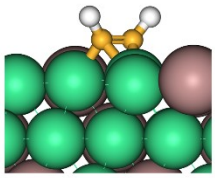	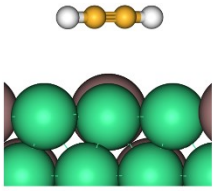
E_{ads} (eV)	**-2.37**	**--2.22**	**-0.14**
G_{ads} (eV)	**-2.06**	**-1.90**	**0.22**

Table S5. Adsorption energies (E_{ads}/eV) and Gibbs free adsorption energies (G_{ads}/eV) of C_2H_4 on the Ni_3Ga (111) surface.

Top View	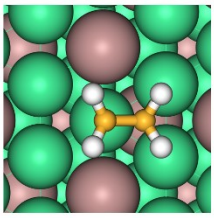	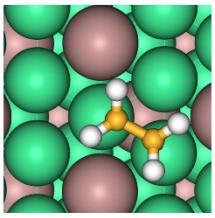
Side View	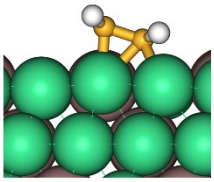	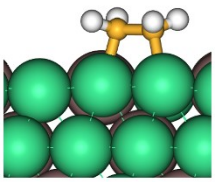
E_{ads} (eV)	**-1.10**	**-0.74**
G_{ads} (eV)	**-0.92**	**-0.52**

Table S6. Adsorption energies (E_{ads}/eV) and Gibbs free adsorption energies (G_{ads}/eV) of C_2H_2 on the Ni(111) surface.

Top View	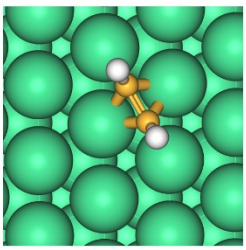	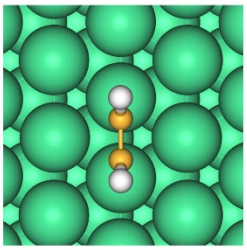	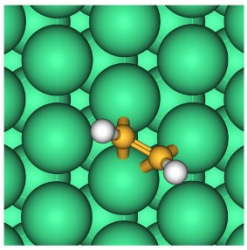
Side View	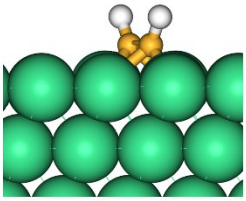	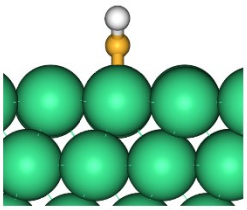	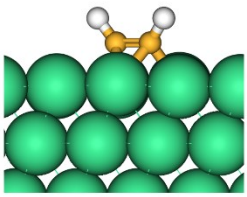
E_{ads} (eV)	**-2.75**	**-1.62**	**-2.36**
G_{ads} (eV)	**-2.45**	**-1.31**	**-2.05**

Table S7. Adsorption energies (E_{ads}/eV) and Gibbs free adsorption energies (G_{ads}/eV) of C_2H_4 on the Ni (111) surface.

Top View	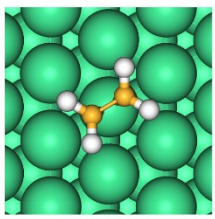	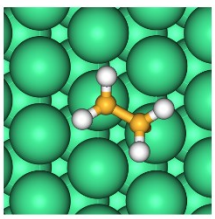	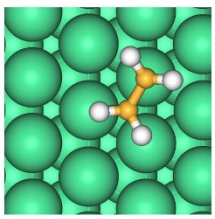	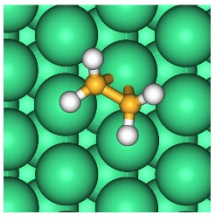
Side View	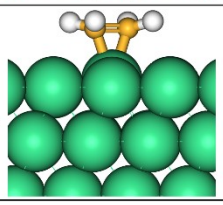	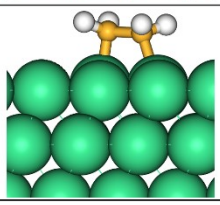	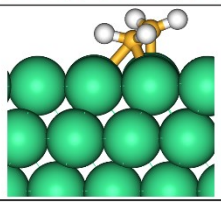	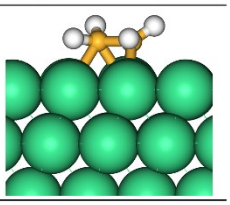
E_{ads} (eV)	**-0.92**	**-0.84**	**-1.00**	**-0.93**
G_{ads} (eV)	**-0.70**	**-0.63**	**-0.82**	**-0.77**

Table S8. Adsorption energies (E_{ads}/eV) and Gibbs free adsorption energies (G_{ads}/eV) of C_2H_4 on the Ni_3Ga (200) surface.

Top View	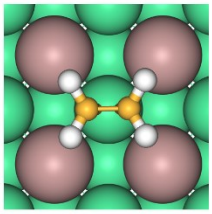	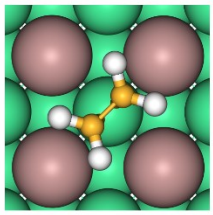	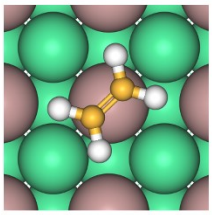	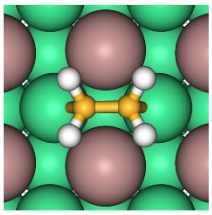
Side View	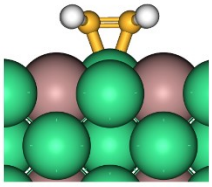	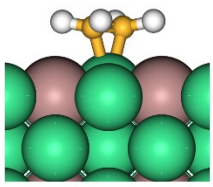	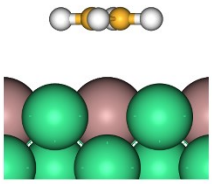	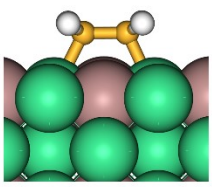
E_{ads} (eV)	**-0.74**	**-0.82**	**-0.13**	**0.15**
G_{ads} (eV)	**-0.50**	**-0.58**	**0.14**	**0.36**

Table S9. Adsorption energies (E_{ads}/eV) and Gibbs free adsorption energies (G_{ads}/eV) of C_2H_4 on the $Ni_3GaC_{0.5}$ (200) surface.

Top View	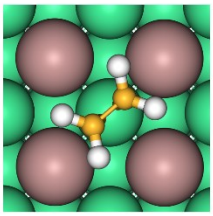	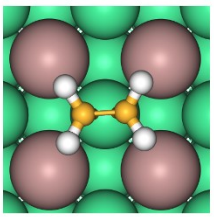	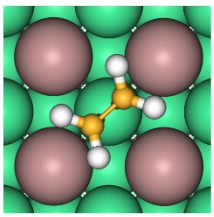	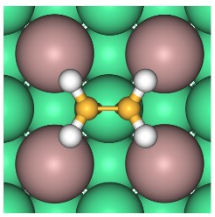
Side View	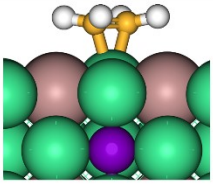	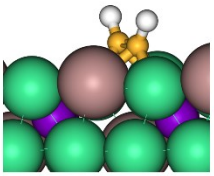	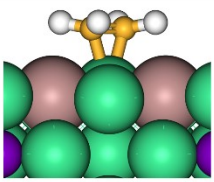	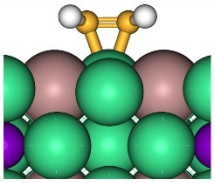
E_{ads} (eV)	**-0.73**	**-0.68**	**-0.70**	**-0.62**
G_{ads} (eV)	**-0.49**	**-0.44**	**-0.45**	**-0.38**

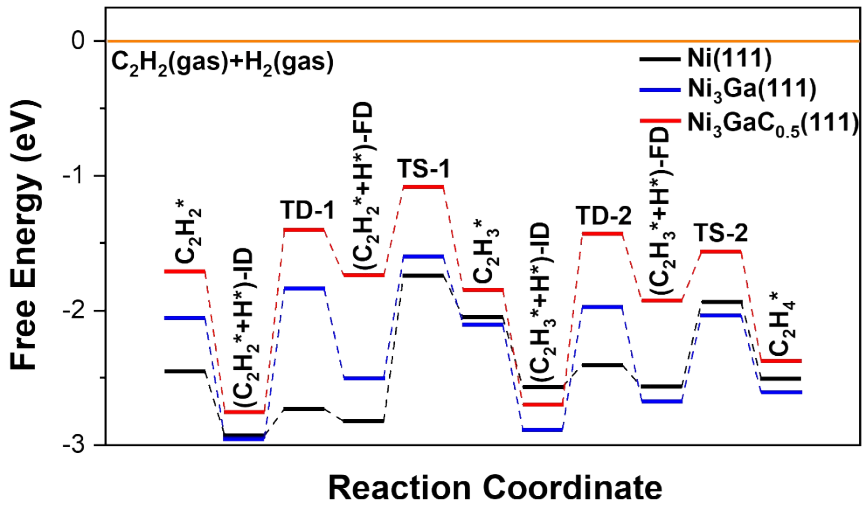

Fig. S23. Energy profiles of the overall acetylene hydrogenation reactions over the Ni(111), $Ni_3Ga(111)$ and $Ni_3GaC_{0.5}(111)$ surfaces.

The turnover frequency (TOF) can be calculated to evaluate the activity. According to the energetic span theory proposed by Sason Shaik et al.[1], the TOF can be calculated by:

$$TOF \approx \frac{k_B T}{h} e^{-G_a^{eff}/RT} \quad (1)$$

where k_B, T and h are the Boltzmann constant, the reaction temperature, and the Planck constant, respectively. G_a^{eff} is the effective barrier of a specific reaction defined as[2, 3]:

$$G_a^{eff} = \begin{cases} G_{TDTS} - G_{TDI} & \text{if TDTS appears after TDI} \quad (a) \\ G_{TDTS} - G_{TDI} + \Delta G & \text{if TDTS appears before TDI} \quad (b) \end{cases} \quad (2)$$

TDTS is the TOF determining transition state related to the hydrogenation step with the highest hydrogenation barrier; TDI stands for the TOF determining intermediate, which is the most stable adsorption state along the energy profile; ΔG is the reaction heat from reactant to TDI.

According to Eq. (1), the G_a^{eff} values at a specific temperature (i.e., 383.15 K in this work) can be employed to compare the difference in hydrogenation activities on the Ni, Ni_3Ga and $Ni_3GaC_{0.5}$, and lower G_a^{eff} indicates higher activity. Along this line, the energy profiles for the hydrogenation of C_2H_2 were calculated and shown in **Fig. S23**. Here, we take the hydrogenation of C_2H_2 on the Ni(111) surface as an example to show how to obtain the G_a^{eff} from the energy profiles (**Fig. S23** and **24**). The first step is to find the TDI intermediate, which is the most stable adsorption state in the energy profile. For the hydrogenation of C_2H_2 on the Ni(111) surface, the TDI is found to be the initial state of C_2H_2 and H co-adsorption, which is denoted as (C_2H_2*+H*)-ID. Then, the second step is to find the elementary step with the highest energy barriers, and the corresponding transition state is the TDTS intermediate. On the Ni(111) surface, the TDTS is found to be the transition state

of the C_2H_2* hydrogenation to C_2H_3* (**Fig. S23** and **S24**). As TDTS appears after TDI, the G_a^{eff} should be calculated according to Eq. 2(a). The value of G_a^{eff} is calculated to be 1.19 eV.

Table S10. The energies of TDTS and TDI, and the calculated G_a^{eff} for hydrogenation of C_2H_2 to C_2H_4 over the Ni(111), $Ni_3Ga(111)$ and $Ni_3GaC_{0.5}(111)$ surfaces.

	Ni(111)	**$Ni_3Ga(111)$**	**$Ni_3GaC_{0.5}(111)$**
TDTS	TS-1	TS-1	TS-1
G_{TDTS} (eV)	-1.74	-1.60	-1.08
TDI	(C_2H_2*+H*)-ID	(C_2H_2*+H*)-ID	(C_2H_2*+H*)-ID
G_{TDI} (eV)	-2.93	-2.95	-2.75
G_a^{eff} (eV)	1.19	1.35	1.67

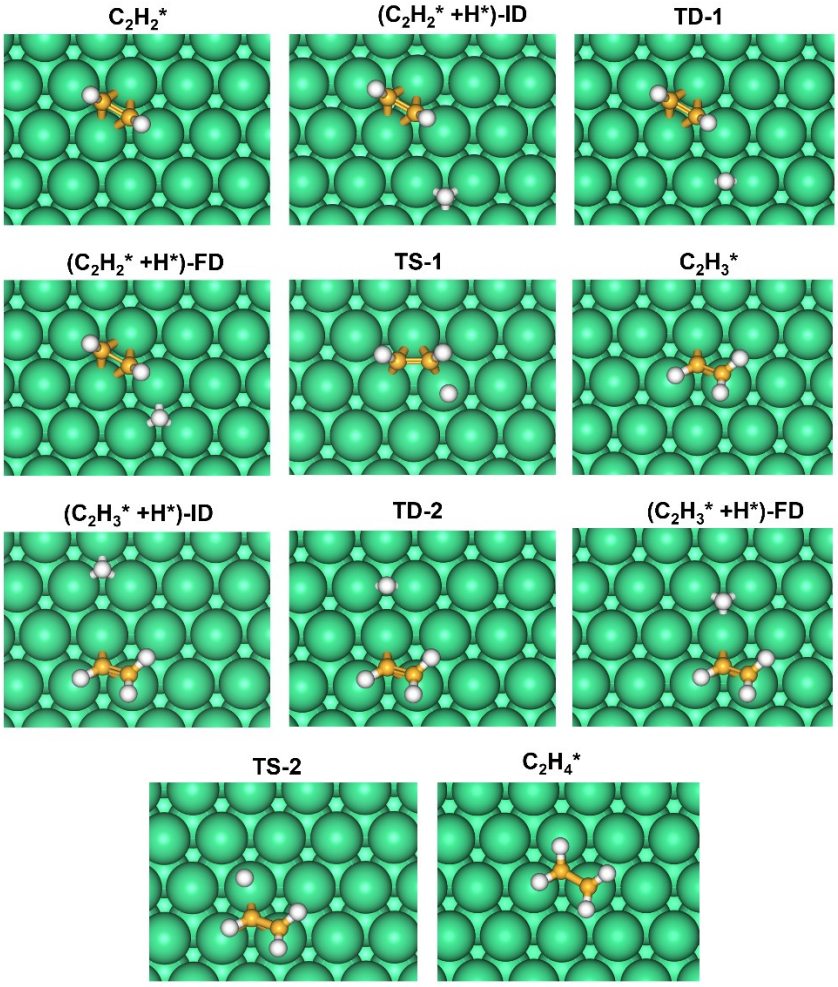

Fig. S24. Configurations of intermediates involved in the hydrogen diffusion and acetylene hydrogenation over the Ni(111) surface. “ID”, “TD” and “FD” stand for the initial states, transition states the final states of the diffusion processes, respectively.

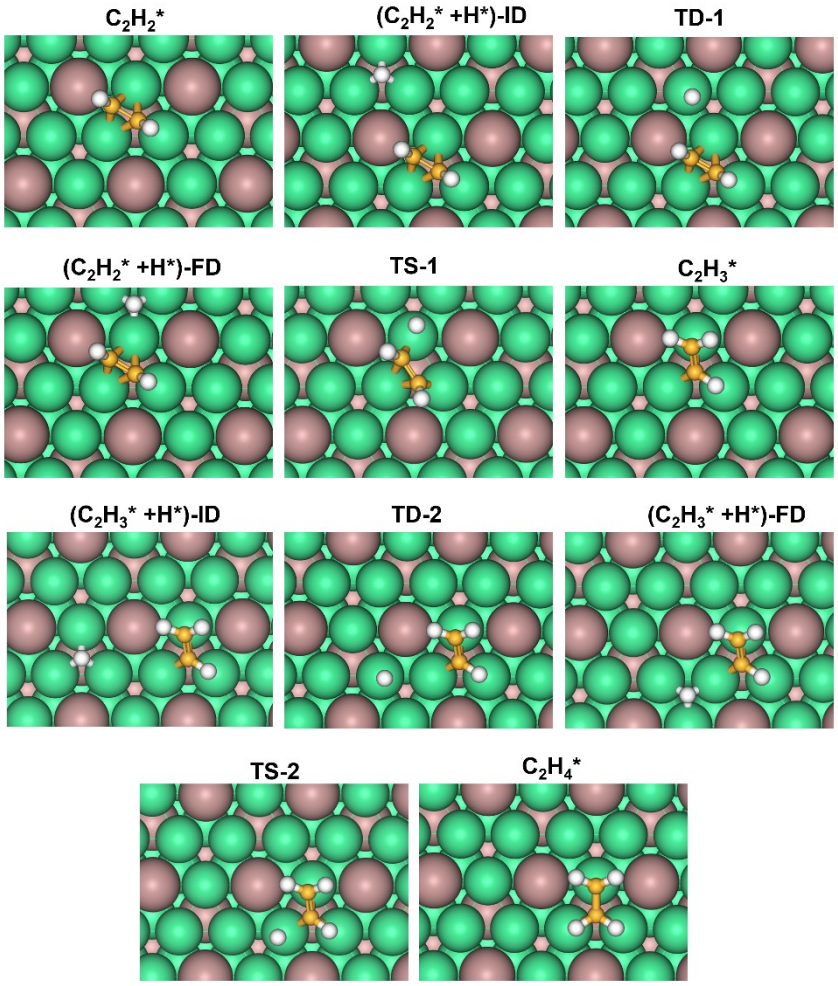

Fig. S25. Configurations of intermediates involved in the hydrogen diffusion and acetylene hydrogenation over the $Ni_3Ga(111)$ surface. "ID", "TD" and "FD" stand for the initial states, transition states the final states of the diffusion processes, respectively.

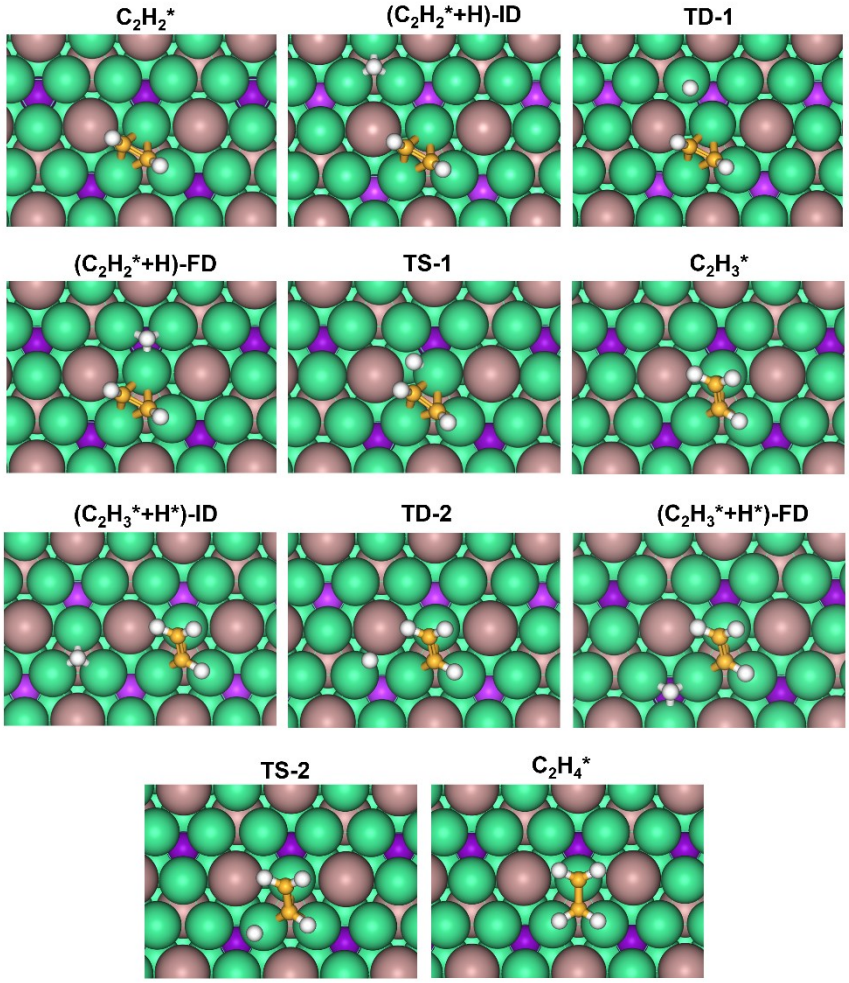

Fig. S26. Configurations of intermediates involved in the hydrogen diffusion and acetylene hydrogenation over the $Ni_3GaC_{0.5}$(111) surface. "ID", "TD" and "FD" stand for the initial states, transition states the final states of the diffusion processes, respectively.

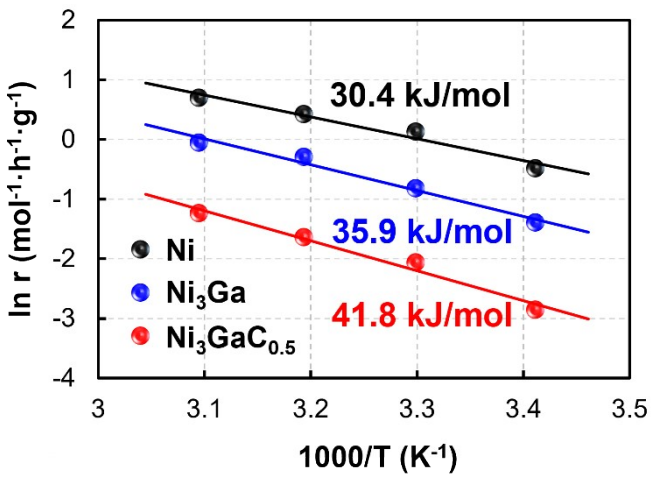

Fig. S27. Arrhenius plots for acetylene conversion over the Ni, Ni_3Ga and $Ni_3GaC_{0.5}$ catalysts.

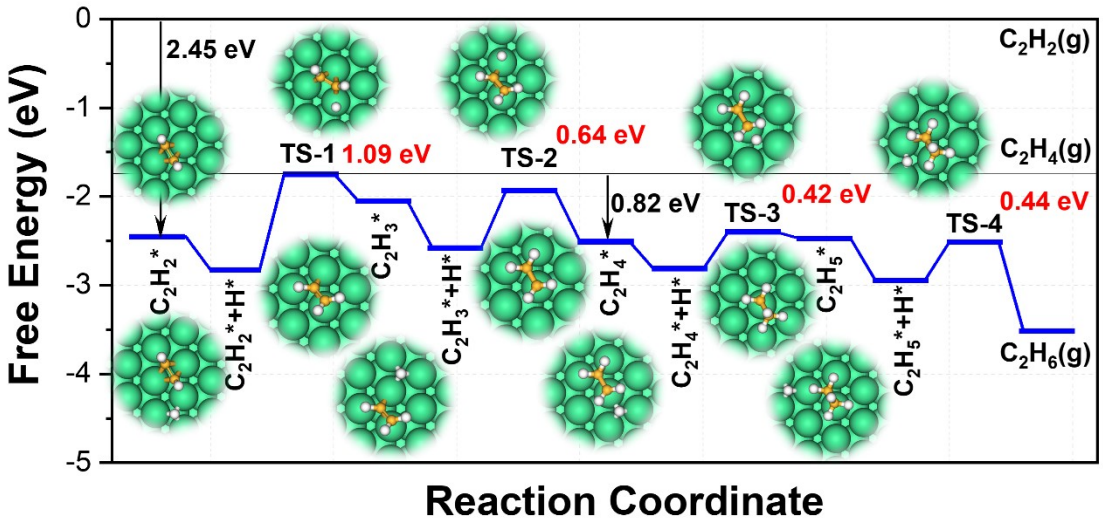

Fig. S28. Free energy profiles for sequential hydrogenation processes of acetylene to ethane on the Ni (111) surface.

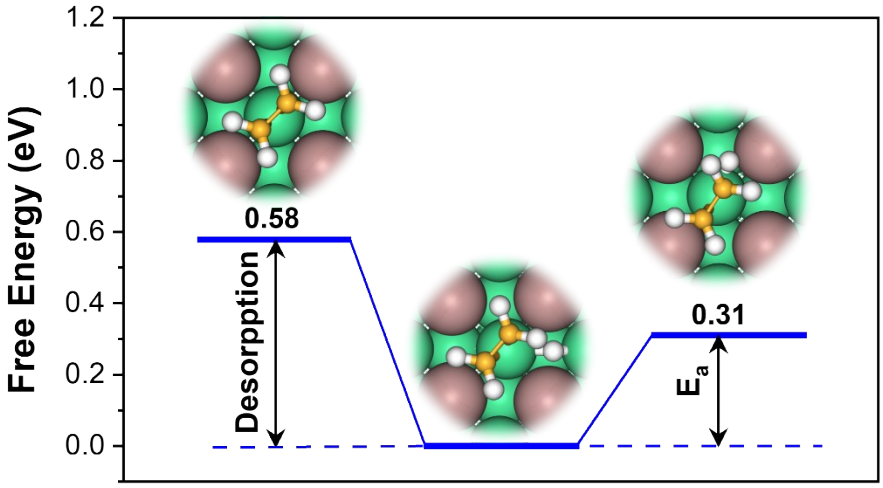

Fig. S29. Free energies for the ethylene desorption versus hydrogenation over the Ni_3Ga (200) surface.

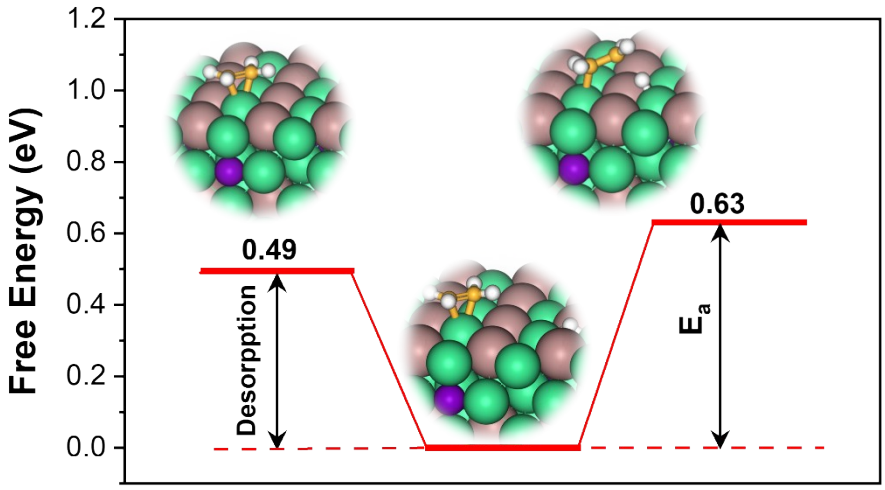

Fig. S30. Free energies for the ethylene desorption versus hydrogenation over the $Ni_3GaC_{0.5}$ (200) surface.

Table S11. Free energies for the ethylene desorption versus hydrogenation over the Ni (111), Ni_3Ga (111), $Ni_3GaC_{0.5}$ (111), Ni_3Ga (200) and $Ni_3GaC_{0.5}$ (200) surfaces.

	G_{des} (eV)	G_a (eV)	ΔG (eV)
Ni (111)	0.82	0.42	-0.40
Ni_3Ga (111)	0.92	0.55	-0.37
$Ni_3GaC_{0.5}$ (111)	0.69	1.18	0.49
Ni_3Ga (200)	0.58	0.31	-0.27
$Ni_3GaC_{0.5}$ (200)	0.49	0.63	0.14

G_{des} and G_a are the desorption free energy of ethylene and the free energy barrier of ethylene hydrogenation, respectively. $\Delta G = G_a - G_{des}$ is employed to estimate the selectivity of ethylene product, and a more positive ΔG value indicates better selectivity to ethylene.

REFERENCES

1. S. Kozuch and S. Shaik, *J. Am. Chem. Soc.*, 2006, **128**, 3355-3365.
2. S. Kozuch and J. M. L. Martin, *ACS Catal.*, 2011, **1**, 246-253.
3. S. Kozuch and S. Shaik, *Acc. Chem. Res.*, 2011, **44**, 101-110.